

NUMERICAL MODELING OF WIRE ELECTROHYDRODYNAMIC FLOW IN A WIRE-PLATE ESP

Young Nam Chun

Department of Environmental Engineering, Chosun University, Korea

Abstract : Numerical modeling of the flow velocity fields for the near corona wire electrohydrodynamic (EHD) flow was conducted. The steady, two-dimensional momentum equations have been computed for a wire-plate type electrostatic precipitator (ESP). The equations were solved in the conservative finite-difference form on a fine uniform rectilinear grid of sufficient resolution to accurately capture the momentum boundary layers. The numerical procedure for the differential equations was used by SIMPLEST algorithm. The Phoenix (Version 3.5.1) CFD code, coupled with Poisson's electric field, ion transport equations and the momentum equation with electric body force were used for the numerical simulation and the Chen-Kim $k-\varepsilon$ turbulent model numerical results that an EHD secondary flow was clearly visible in the downstream regions of the corona wire despite the low Reynolds number for the electrode ($Re_{cw}=12.4$). Secondary flow vortices caused by the EHD increases with increasing discharge current or EHD number, hence pressure drop of ESP increases.

Key Words : Electrodynamics, Electrostatic Precipitator, EHD turbulent modeling, Von-Karman type vortex

INTRODUCTION

Industrial electrostatic precipitation (ESP) has a very complex interaction between the electric field gas and particulate flows. The motion and precipitation of dust particles in an ESP depends on the electric field, space charge, gas flow field and dust particle properties.

A several investigation^{1,2)} estimated EHD flow effects on the dust particle collections may be significant. However, it is still unclear whether these EHD turbulent flow structures enhances or deteriorates fine particle precipitation processes. EHD turbulence can be generated, even for Reynolds number less than 1, if the EHD number (Ehd) is sufficiently large enough than the square

of the critical Reynolds number ($Ehd > Re^2$).³⁾

Yamamoto and Velkoff¹⁾ performed numerical calculations to solve the two dimensional Navier-Stokes equations governing fluid flow with the electric field and ion distribution. Turbulent EHD analyses have been carried out to calculate the EHD flow field by solving the time-averaged Navier-Stokes equations, using $k-\varepsilon$ turbulence closure⁴⁾, RNG $k-\varepsilon$ ⁵⁾ and Reynolds stress models.⁶⁾ Although these turbulence models have previously been successfully applied in same cases, yielding what were assumed to be reasonable results for practical ESP conditions, the validity of these turbulence models for ESP applications due to the isotropic assumption and/or their difficulty in showing small eddy effects, as they only appear useful for models with a high Reynolds number still under investigation with experimental validations.

The physical mechanism of EHD flow is based

[†] Corresponding author

E-mail: ynchun@chosun.ac.kr

Tel: +82-62-230-7156, Fax: +82-62-230-7156

on a model, where the ion produced by the corona discharge near to the corona wire will be transported toward the grounded wall due to the Coulomb force. The ions provide a bulk body force to the fluid flow, resulting from the collision between the ions and neutral molecules. The body force causes the flow field to become complicated, as expressed by the product source of the space charge density and the electric field strength in the momentum equation.⁷⁾

Although there have been many experimental investigations on the particle transport in ESPs, so far only a few have directly measured the flow field inside the precipitation zone without disturbing electric field or flow. However, non intrusive optical techniques such as laser Doppler velocimeter (LDV) and particle image velocimeter (PIV) become available for EHD-ESP flow investigations. These results show EHD secondary flow not only generates large wake near grounded plate but also formed behind corona wire.⁸⁾

In the present study, a turbulent low/high Reynolds number model was used to investigate EHD flow, particularly the wake downstream near the corona wire. Furthermore, the mechanisms of the EHD secondary flow (ionic wind) were modeled by this selected Chen-Kim modified $k-\varepsilon$ turbulent model.⁹⁾

NUMERICAL SIMULATION

General Simulation Procedure

Numerical studies were performed for a wire-plate electrostatic precipitator. The corona discharge wire, 0.9 mm in diameter, was placed in the center of the horizontal parallel plate electrodes. The lengths of the plate electrodes were 60 cm and a gap distance between two plates is 10 cm as shown in Figure 1.

Steady-state two-dimensional fields were assumed to simplify the physical phenomena. The turbulent fluid flow within an ESP was calculated using the commercially available Phoenics (Version 3.5.1) CFD code, with a finite volume method for the time-averaged Navier-Stokes equations closed by the $k-\varepsilon$ turbulent model. The numerical procedure

for the differential equations was used by SIMPLEST¹⁰⁾ algorithm. A laminar model was also used to calculate the laminar flow without an EHD flow.

The ion charge density, electric field and space charge terms of the momentum equations were programmed into the user defined subroutines of the Phoenics code. The governing equations for the EHD flow field (u_i, k, ε) and electrical parameters (E_r, N_c) were solved by iterative solvers, which were cycled through the equation sequence of the global iteration for coupling between the equations.

Flow Modeling for EHD Flow

Experimental results¹¹⁾ have shown that the corona induced-turbulence is significant when $Ehd \geq Re^2$ and turbulent EHD initiated near the corona wire.^{3,12)} Hence, in this work, unlike the previous works based on the laminar flow model, the $k-\varepsilon$ turbulence model was chosen.

In this work, the Chen-Kim modified $k-\varepsilon$ turbulent model, which has low and high Reynolds models, was chosen since it was most effective for turbulent EHD flow near the corona wire, as it can show small eddy effects of the bulk body, such as the Von-Karman vortex in the rear flow of the wire.³⁾

Electric Field and Space Charge Distribution

Analytical model of Thompson¹²⁾ corona discharge in a coaxial wire-tube electrode geometry was used for electric field and ion density distribution. The strength of the electric field and the ion charge density were determined using Poisson's (Eq. (1)) and the ion transport equations (Eq. (2)) for cylindrical coordinate as follows:

$$\frac{1}{r} \frac{d(rE_r)}{dr} = -\frac{eN_c}{\varepsilon} \quad (1)$$

$$\frac{I_c}{2\pi rL} = e(U_{gr} + \mu_c E_r)N_c \quad (2)$$

where E_r is the electric field, r the radius, N_c the number of ions, e the electric elementary

charge ($=1.6021892 \times 10^{-19}$ C), ϵ the dielectric constant ($=8.85418782 \times 10^{-12}$ F/m), I_c the current, L the plate depth, U_{gr} the mean gas velocity and μ_c the mobility ($=0.0002546$ cm²/Vs).

By integrating Eq. (1), the strength of the electric field is expressed as:

$$E_r = \left(\frac{I_c}{2\pi\epsilon\mu_c L} + \frac{C_0^2}{r^2} \right)^{0.5} \quad E_r = -\frac{dV}{dr} \quad (3)$$

where C_0 is the integration constant calculated from the experimental current-voltage characteristics in Tables 1 and 2.¹³⁾

The ion number then yield:

$$N_c = \frac{I_c}{e 2\pi r L (U_{gr} + \mu_c E_r)} \quad ; \quad \rho_{ion} = e N_c \quad (4)$$

We assumed that electric field and ion density in wire-plate ESPs can be calculated from Eqs. (3) and (4) except electric potential at corona wire $V = V_p$ and at grounded plate $V = 0$.

EHD Flow Field

For a steady-state incompressible turbulent flow, the continuity and momentum equations can be written as:

$$\frac{\partial}{\partial x_i} (\rho u_i) = 0 \quad (5)$$

$$\frac{\partial}{\partial x_j} (\rho u_i u_j) = -\frac{\partial p}{\partial x_i} + \frac{\partial}{\partial x_j} \left[(\mu + \mu_t) \left(\frac{\partial u_i}{\partial x_j} + \frac{\partial u_j}{\partial x_i} \right) - \rho \overline{u_i' u_j'} \right] + \rho_{ion} E_i \quad (6)$$

where u is the fluid mean velocity, p the mean static pressure, μ_t the turbulent eddy viscosity, u' the fluctuation velocity, ρ_{ion} the ion charge density and E_i the strength of the electric field. The electric field strength and ion charge density are calculated from Eqs. (3) and (4), respectively.

Using the Boussinesque eddy-viscosity hypothesis, the Reynolds stress tensor is expressed as:

$$-\rho \overline{u_i' u_j'} = \mu_t \left(\frac{\partial u_i}{\partial x_j} + \frac{\partial u_j}{\partial x_i} \right) - \rho k \frac{2}{3} \delta_{ij} \quad (7)$$

where δ_{ij} is the Kronecker delta.

The turbulent eddy viscosity is:

$$\mu_t = \rho C_\mu \frac{k^2}{\epsilon} \quad (8)$$

so is calculated from the solution of the conservation equations of the turbulent kinetic energy (k) and the turbulent dissipation rate (ϵ) in the standard $k-\epsilon$ model (hereafter referred to as KE).¹⁴⁾

The $k-\epsilon$ model employs a single time scale (k/ϵ) to characterize the various dynamic processes that occur in turbulent flows. Turbulence ; however, is comprised of fluctuating motions, with a spectrum of time scales, and a single-scale approach is unlikely to be adequate under all circumstances, as different turbulence interactions are associated with different parts of the spectrum. In order to remedy this deficiency in the standard model, Chen and Kim⁹⁾ proposed a modification that improves the dynamic response of the ϵ equation. The Chen Kim modified $k-\epsilon$ turbulent model (referred to as CK) should be proposed as both low and high Reynolds number models.

In addition, low Reynolds number models were used by Lam-Bremhorst low-Re extension to the $k-\epsilon$ model (LB),¹⁵⁾ 'Yap' correction for separated flows (YAP),¹⁶⁾ and high Reynolds number models were used by RNG derived $k-\epsilon$ turbulence model (RNG)¹⁷⁾ to compare the different models.

Turbulent intensity was calculated using the following equation:

$$I_T = \frac{\sqrt{\overline{(u')^2}}}{U_0} \quad (9)$$

The fluctuation velocity, u' , is calculated from the turbulent kinetic energy, as $k = 1.5u'^2$, obtained from Eq. (8) with the isotropy assumption.

The dimensionless EHD number and the Reynolds number at the plate and the wire were calculated by bellow definitions.¹⁸⁾

The EHD numbers at the flow channel and wire are defined as follows:

$$Ehd_{FC} = \frac{I_0 L^3}{\rho_f \nu_f^2 \mu_i A} \quad \text{at the flow channel,} \quad (10)$$

$$Ehd_{CW} = \frac{I_0 d^3}{\rho_f \nu_f^2 \mu_i A} \quad \text{at the wire}$$

where I_0 is the reference current, L the characteristic length, ρ_f the fluid density, ν_f the fluid kinematic viscosity, μ_i the mobility, A the surface area and d the wire diameter.

The Reynolds numbers at the plate and wire are defined as follows:

$$Re_{FC} = \frac{Lu_0}{\nu_f} \quad \text{based on the flow channel plate at plate distance,} \quad (11)$$

$$Re_{CW} = \frac{du_0}{\nu_f} \quad \text{based on the wire diameter}$$

where u_0 is the gas flow velocity.

Boundary conditions used in the present study are shown in Figure 1. Inlet velocity is used velocity profile as bellow;

$$u = u_0 \left[1 - \left(\frac{y}{y_p} \right)^2 \right] \quad (12)$$

The electric potential and velocity are $V = V_p$, $u=0$ at corona wire and $V=0$, $u=0$ at grounded plate, respectively.

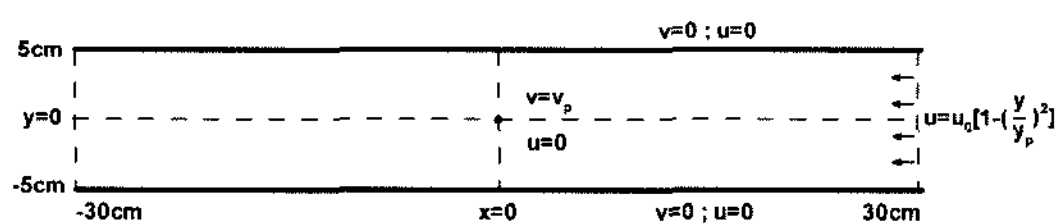


Figure 1. Boundary conditions used in the present calculations.

RESULT AND DISCUSSION

Current-Voltage Characteristics

Currents and voltages were experimentally obtained according to various gas velocity and EHD numbers by using single wire-plate ESP test rig.⁸⁾ Table 1 summarizes currents and voltages gas flow

velocity 0.2 m/s ($Re_{CW}=12.4$ at corona wire, $Re_{FC}=1,377$ at flow channel), and Table 2 summarizes current and voltage ($Ehd_{CW}=1.31 \times 10^6$, $Ehd_{FC}=4.04 \times 10^2$) for various gas velocity.

Table 1. Experimentally measured current-voltage characteristics for mean velocity at 0.2m/s ($Re_{CW}=12.4$, $Re_{FC}=1,377$)

Case	Voltage (kV)	Current (μA)	Ehd _{CW}	Ehd _{FC}
Laminar	0	0	0	0
E1	+19.9	20	1.31×10^6	4.04×10^2
E2	+22.2	30	1.96×10^6	6.06×10^2
E3	+24.1	40	2.61×10^6	8.08×10^2
E4	+25.1	60	3.92×10^6	1.21×10^3
E5	+29.1	90	5.88×10^6	1.82×10^3

Table 2. Experimentally measured current-voltage characteristics for EHD number at $Ehd_{FC}=1.31 \times 10^6$ and $Ehd_{CW}=4.04 \times 10^2$

Case	Mean Velocity (m/s)	Voltage (kV)	Current (μA)	Re_{CW}	Re_{FC}
v0.2	0.2	+19.9	20	12.4	1,377
v0.5	0.5	+20.8	20	31.0	3,441
v0.8	0.8	+20.3	20	49.6	5,506
v1.0	1.0	+20.8	20	61.9	6,882

Effect of EHD Number

An experimental investigation has been conducted for EHD flow study in ESP by particle Image velocimeter(PIV) with ESP geometry as shown in Figure 1. The current-voltage characteristics observed by Mizeraczyk et al¹⁹⁾ for the primary flow velocity at 0.2 m/s is summarized in Table 1. The results of the PIV measurement are analyzed in terms of EHD number as defined in Eq.(10). These geometry and experimental values are used for the present numerical simulation.

Figure 2. shows the flow distribution for various applied voltages or EHD number.

Without an applied voltage, 0 kV, for which the EHD numbers based on the corona wire and flow channel are $Ehd_{CW}=0$ and $Ehd_{FC}=0$, respectively, "Laminar" in Figure 2. shows the usual laminar flow in the channel, as would be expected from Reynolds numbers of $Re_{CW}=12.4$ and $Re_{FC}=1,377$. However, once the EHD numbers increase

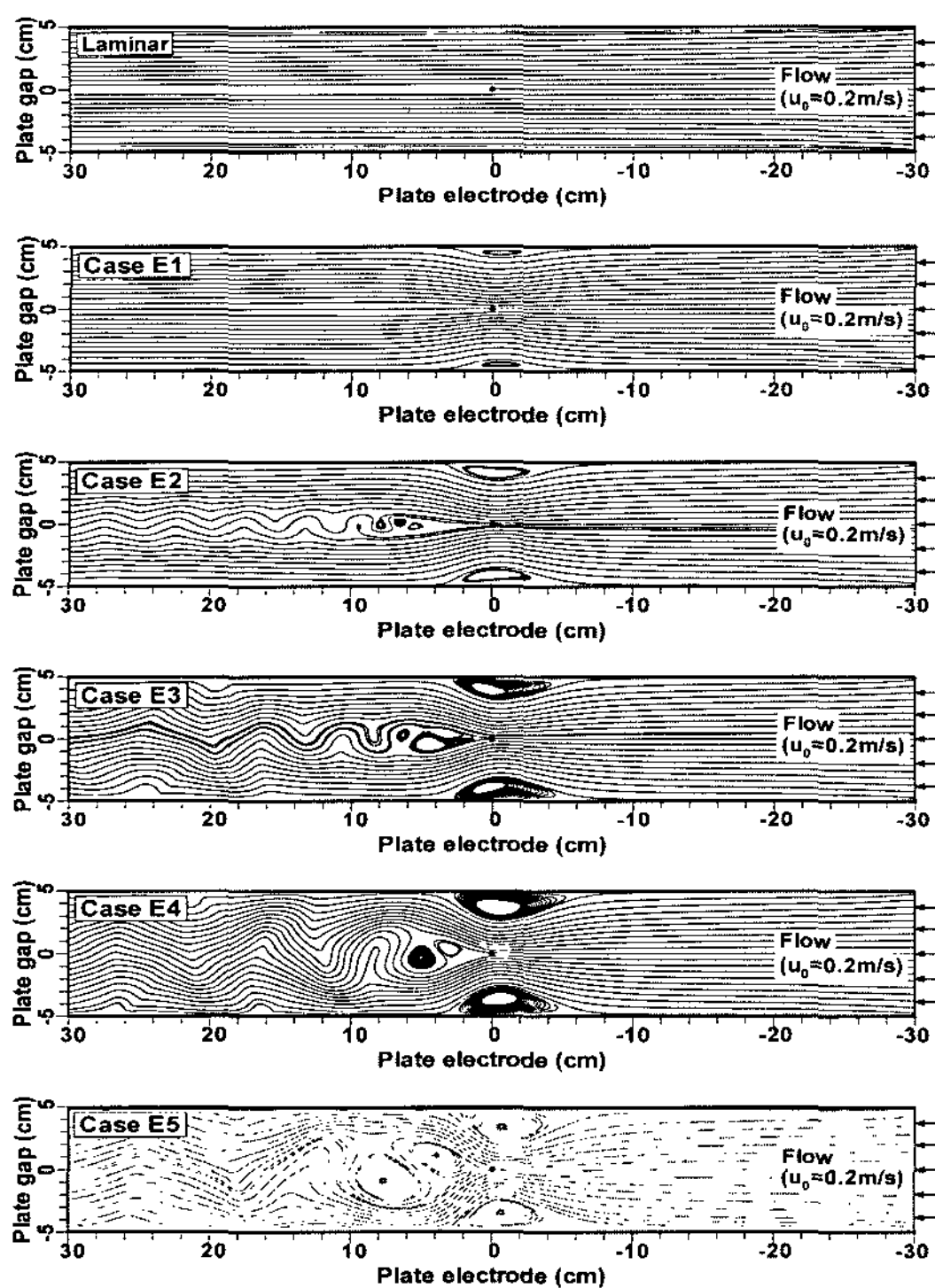


Figure 2. Flow streamlines in a wire-plate electrostatic precipitator for various EHD numbers at entrance mean flow velocity 2m/s ($Re_{CW}=12.4$ and $Re_{FC}=1,377$).

from $Ehd_{CW}=1.31 \times 10^6$ to $Ehd_{CW}=5.88 \times 10^6$, not only were unsteady wakes observed, but forward wakes were also evident. Particularly, the so called Von-Karman vortex stream was observed for $Ehd_{CW}=1.96 \times 10^6$, and with increases in EHD number, such as $Ehd_{CW}=2.61 \times 10^6$ through $Ehd_{CW}=5.88 \times 10^6$, the downstream vortices in the channels were fully developed.

As the applied voltage increases, the greater the amount of flow interaction takes place. For $Ehd_{CW}=5.88 \times 10^6$, it was clear that the gas entering the channel gradually accelerated, being deflected towards the center line of the channel due to the EHD secondary flow (i.e., ionic wind or electric wind). The level of this EHD generated turbulence was significant as there were strong interactions between the electric field, the electric charge and the gas flow. The investigation of the near-collection electrode region shows the importance of the secondary vortex flow. This means that secondary flows can have a great impact on

the motion and precipitation of small particles, mainly those in the submicron range.¹⁹⁾

Figure 3. shows streamwise velocity profiles along the symmetry line, via the corona wire, with no applied voltage and with different applied voltages for the flow velocity, $u_0=0.2$ m/s. When $Ehd=0$, the velocity was only slightly changed at the outlet. However, the character of the flow changed dramatically after a voltage was applied ($Ehd \neq 0$), with the flow becoming turbulent and showing many different turbulent structures, as explained in Figure 2.

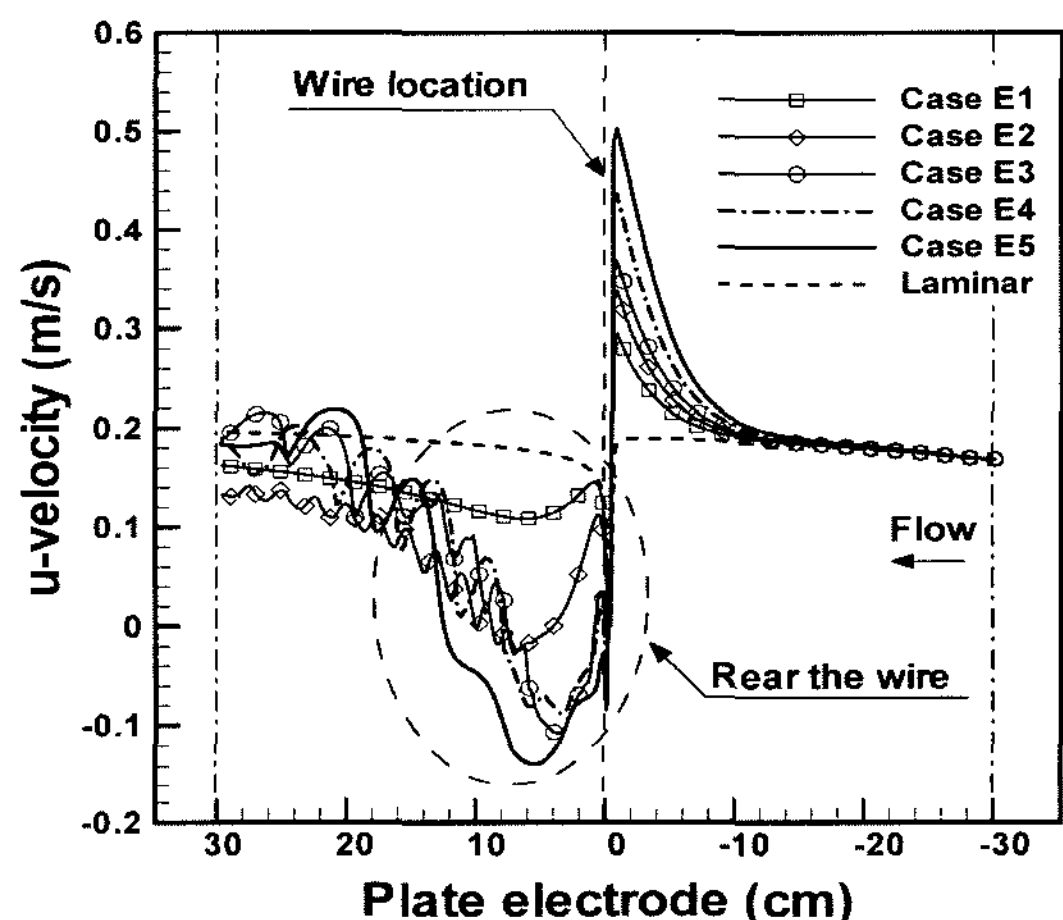


Figure 3. Streamwise velocities along the axis of ESPs for various EHD numbers at entrance velocity 0.2m/s.

The gas velocity near the corona wire increase close to the front of the wire, however significantly decrease at the rear of the wire as the EHD number was increased. This was caused by the EHD flow induced by the electric body force of ions. The increasing velocity at the front wire is due to the increase in the counter flow to compensate for the vertical bulk flow, which travels in the direction of the plate electrode from the wire. Otherwise, the decrease at the rear wire is due to the streamwise velocity being decreased by the flow reversal. Particularly, in the case of $Ehd > 2 \times 10^6$, the velocities had negative values and may fluctuate due to the large flow turbulence.

Figure 4. shows pressure drop of ESP and EHD induced maximum velocity to primary velocity ratio as a function of the flow channel

EHD numbers (Ehd_{FC}) at same primary velocity 0.2 m/s ($Re_{FC}=1,377$). Pressure drop, $P_{inlet} - P_{outlet}$, is the difference between inlet and outlet pressure, and maximum velocity ratio, u_{max}/u_0 , is the value of maximum streamwise u-velocity divided by flow primary velocity. Figure 4. shows that pressure drop increased gradually with increasing EHD number.

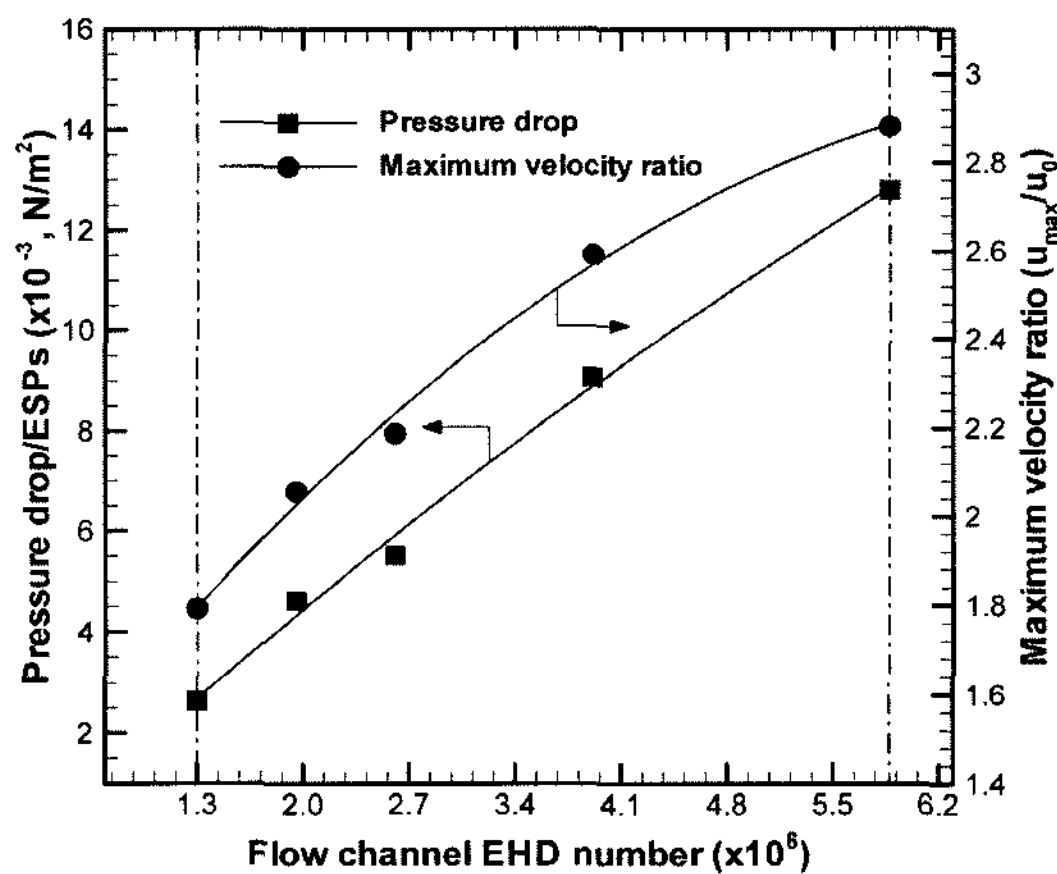


Figure 4. Pressure drops/ESP and EHD enhanced maximum velocity ratios as a function of EHD numbers at $Re_{FC}=1,377$.

Effects of Primary Reynolds Number

The velocity contour for different Reynolds number or gas flow velocity at inlet is shown in Figure 5 for $Ehd_{FC}=4.04 \times 10^2$.

When the gas flow velocity increase from $u_0=0.2$ m/s to $u_0=0.8$ m/s, EHD secondary flow will be decrease due to large primary velocity.

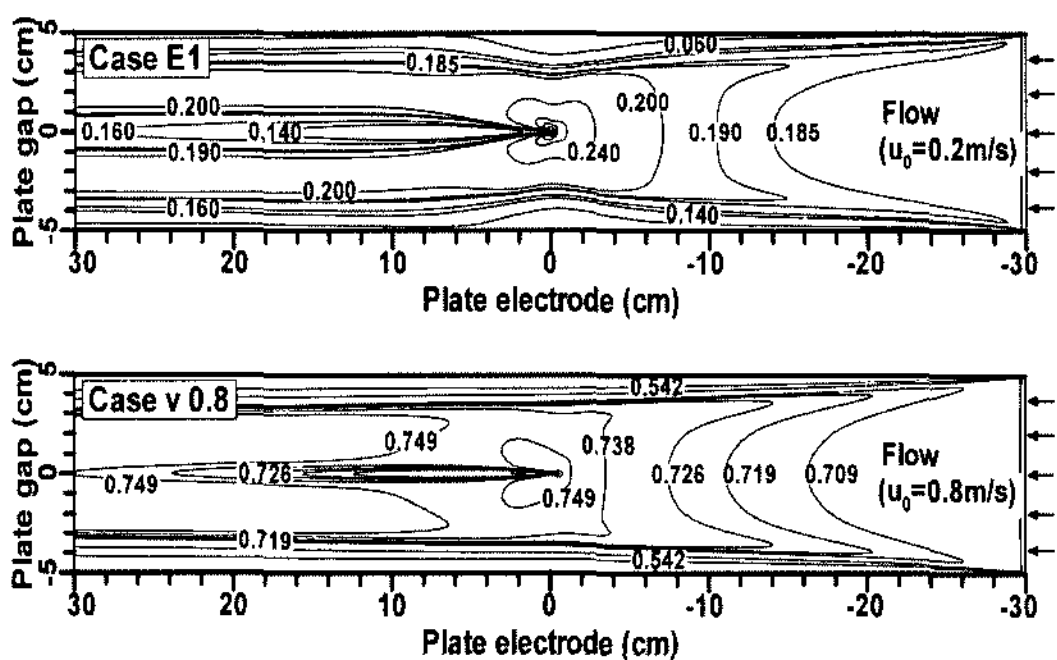


Figure 5. Velocity contours for a wire-plate ESPs for entrance velocity at 0.2m/s and 0.8m/s at EHD number $Ehd_{FC}=4.04 \times 10^2$.

Figure 6 shows the u-velocity, v-velocity and turbulence intensity profiles along the symmetry line, normal to the wall of the plate electrode. As expected, the u-velocity increase with increasing in the primary flow velocity, however the v-velocity decrease, especially near the corona wire. The intensity of the turbulence increases with high flow velocity, for $Re=3,677$, where the turbulence intensity increases significantly near wall due to the small eddy produced by friction resistance at the wall. Otherwise, for low u-flow velocity the turbulence intensity near the wire is larger than near the wall due to the bulk body force produced by the secondary flow as shown in Figure 5.

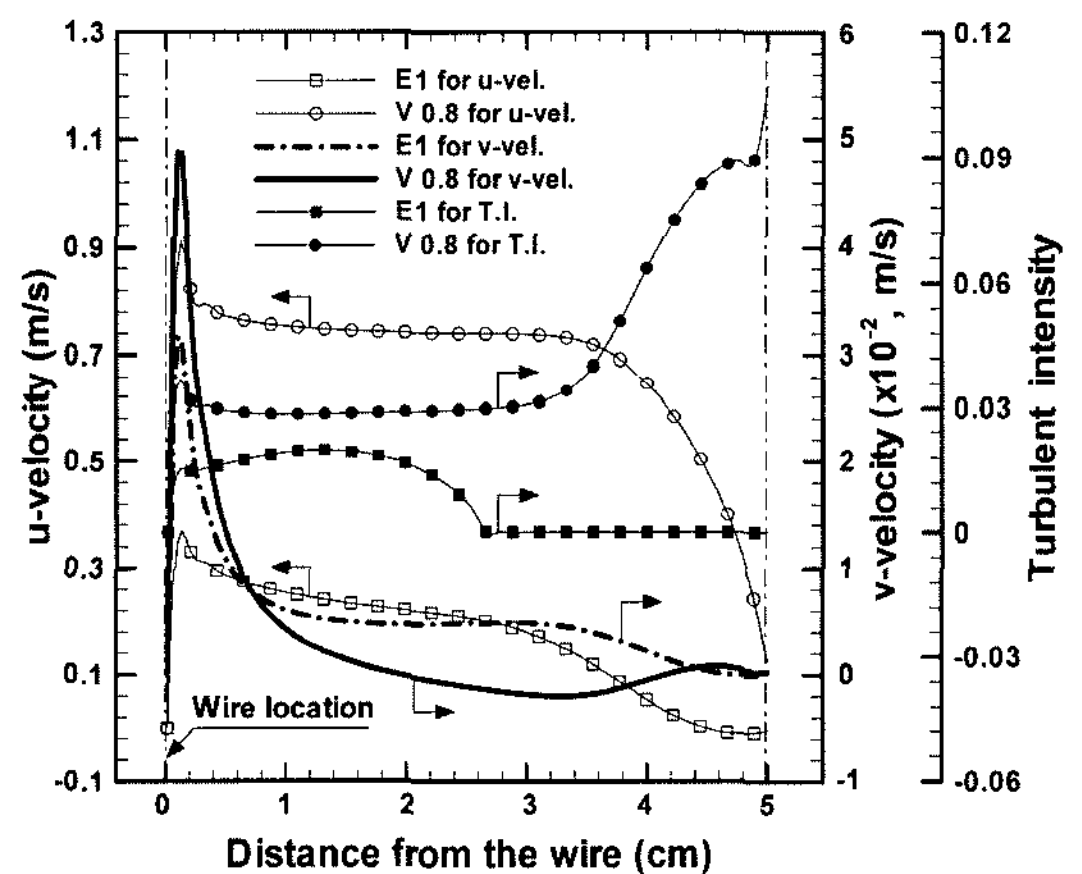


Figure 6. Component velocities and turbulence intensities profiles along the y-axis at $x=0$ (location of corona wire).

The velocity patterns near the corona wire are shown for various EHD numbers in Figure 7.

For lower EHD number flow, as shown in Figure 5, the width of the backward band flow at the rear wire was only increased by the EHD secondary flow. However, for higher EHD number the velocity vectors show a strong EHD secondary flow, which is clearly visible in the downstream regions of the corona wire, despite the low Reynolds number of the electrode ($Re_{CW}=12.4$). The secondary flow vortices are also caused by the EHD when the applied voltage is increased. The expected life span of the ESP, particularly the corona wire, should be shortened by the

vibration produced by the irregular bulk motion in the channels of a commercial ESP.

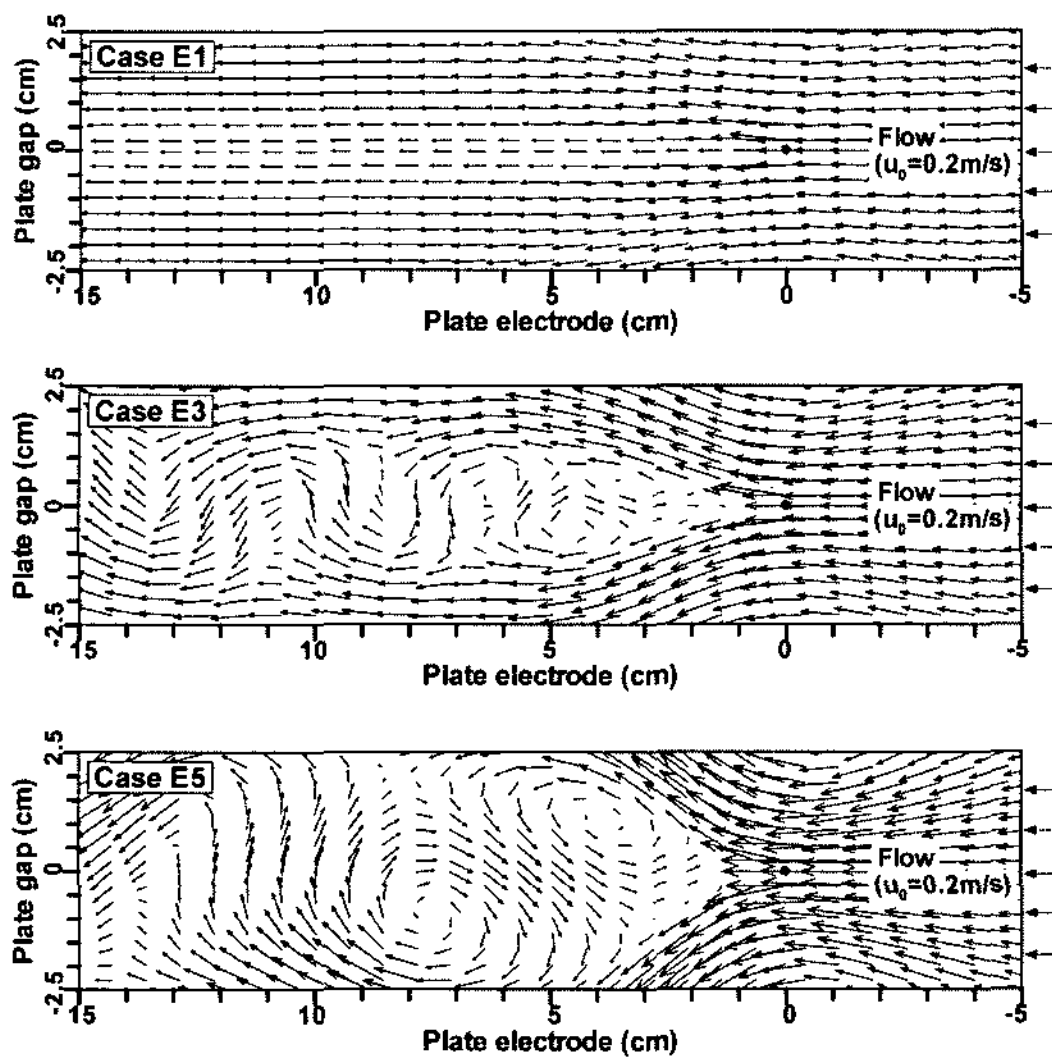


Figure 7. Velocity vectors of the near wire in the ESP.

CONCLUDING REMARKS

The numerical simulations have been used for EHD flow in wire-plate type ESPs and the following concluding remarks are obtained:

- 1) The flow interaction took place when a voltage was on-set. The inflow gas was gradually accelerated, and then deflected towards the center line of the channel due to the secondary flow produced by EHD forces.
- 2) Once EHD numbers have been increased, not only were wakes observed behind corona wires, but some forward wakes were also evident. Particularly, the so called Von-Karman vortex stream was observed at $Ehd_{cw}=1.96 \times 10^6$. Also with the increase in the EHD number, as with $Ehd_{cw}=2.61 \times 10^6$, 3.92×10^6 and 5.88×10^6 , the vortices in the rear flow channel were fully developed.
- 3) Electrohydrodynamically introduced secondary flow exists, not only near the dust collection electrodes, but were also observed near the corona wire. By applying a high voltage, the field velocity pattern shows a strong EHD secondary flow, which is clearly visible in

the downstream regions of the corona wire, despite the low Reynolds number ($Re_{cw}=12.4$). Vortices are also caused by the EHD secondary flow when the applied voltage is increased. Therefore, for flow patterns near the corona wire may contaminate wires due to the EHD wake flow and part of the dust transported outside of the ESPs.

- 4) The EHD secondary flow may be imparting momentum to channel flow, thus increasing the pressure drop.
- 5) The structure of the EHD secondary flow was similar for primary inflow velocities that were sufficiently high compared to the secondary flow itself.

REFERENCES

1. Yamamoto, T. and Velkoff, H. R., "Electrohydrodynamics in an electrostatic precipitator," *J. Fluid Mech.*, **108**, 1-12 (1981).
2. Liang, W. J. and Lin, T. H., "The Characteristics of Ionic Wind and Its Effect on Electrostatic Precipitators," *Aerosol Sci. Technol.*, **20**, 330-336 (1994).
3. Chang, J. S., Brocilo, D., Urashima, K., Dekowski, J., Podlinski, J., Mizeraczyk, J. and Touchard, G., "On-Set of EHD Turbulence for Cylinder in Cross Flow Under Corona Discharges," in Proceedings of the 5th International EHD workshop, 30-31 August, Poitiers, France, pp. 26-31 (2004).
4. Choi, B. S. and Fletcher, C. A. J., "Computation of particle transport in an electrostatic precipitator," *Journal of Electrostatics*, **40**(41), 413-418 (1997).
5. Park, S. J., and Kim, S. S., "Electrohydrodynamic Flow and Particle Transport Mechanism in Electrostatic Precipitators with Cavity Walls," *Aerosol Science and Technology*, **33**, 205-221 (2000).
6. Hans-Joachim Schemid, Steffen Stolz and Hans Buggisch., "On the Modelling of the Electro-Hydrodynamic Flow Field in Electrostatic Precipitators Flow," *Turbulence and Combustion* **68**, 63-89 (2002).

7. Liang, W. J., and Lin, T. H., "The Characteristics of Ionic Wind and its Effect on Electrostatic Precipitators," *Aerosol Sci. Tech.*, **20**, 330-344 (1994).
8. Podlinski, J., Dekowski, J., Mizeraczyk, J., Brocilo, D and Chang, J. S., "Electrohydrodynamic gas flow in a positive polarity wire-plate electrostatic precipitator and the related dust particle collection efficiency," *J. Electrostatics*, **64**, 259-262 (2006).
9. Monson, D. J., Seegmiller, H. L., McConaughy, P. K. and Chen, Y. S., "Comparison of experimental with calculations using curvature-corrected zero and two-equation turbulence models for a two-dimension U-duct," AIAA-90-1484, Fluid Dynamics, Plasma Dynamics and Lasers Conference, Seattle, WA, p. 19 (1990).
10. F. Michel., "New Features of MIGAL solver," in Proceedings of the 9th International PHOENICS User Conference, Moscow, Russia, pp. 23-27 (2002).
11. Riehle, C. and Löffler, F., "Grade Efficiency and Eddy Diffusivity Models," *J. Electrostatics*, **34**, 401-413 (1995).
12. Ohkubo, T., Hamasaki, S., Nomoto, Y., Chang, J. S. and Adachi, T., "The effect of corona wire heating on the downstream ozone concentration profiles in an air-cleaning wire-duct electrostatic precipitator," *IEEE Trans. Indust. Appl. Soc.*, **22**, 542-549 (1990).
13. Thompson, J. J., "Conduction of Electricity through Gases," The Cambridge University Press., New York, p. 267 (1945)
14. Launder, B. E. and Spalding, D. B., "The numerical computation of turbulent flows," *Computer Methods in Applied Mech. and Eng.* **3**, 269-289 (1974).
15. Patel, V. C., Rodi, W. and Scheurer, G., "Turbulence models for near-wall and low-Reynolds-number flows: A review," *AIAA J.*, **23**(9), 1308-1319 (1985).
16. Yap, C., "Turbulent heat and momentum transfer in recirculating and impinging flows," PhD Thesis, Faculty of Technology, University of Manchester, (1987).
17. Yakhot, V. and Orszag, S.A., "Renormalization group analysis of turbulence," *J. Sci. Comput*, **1**, 3 (1986).
18. IEEE-DEIS-EHD Technical Committee, "Recommended International Standard For Dimensionless Parameters Used In Electrohydrodynamics," *IEEE Transactions on Dielectrics and Electrical Insulation*, **10**(1), 3-6, (2003).
19. Mizeraczyk, J., Kocik, M., Dekowski, J., Dors, M., Podliński, J., Ohkubo, T., Kanazawa, S. and Kawasaki, T., "Measurements of the velocity field of the flue gas flow in an electrostatic precipitator model using PIV method," *Journal of Electrostatics*, **51**(52), 272-277 (2001).